Self-Healing Ability of Epoxy Vitrimer Nanocomposites Containing Bio-Based Curing Agents and Carbon Nanotubes for Corrosion Protection

Narubeth Lorwanishpaisarn
Khon Kaen University
Natwat Srikhao
Khon Kaen University
Kaewta Jetsrisuparb
Khon Kaen University
Jesper T.N. Knijnenburg
Khon Kaen University
Somnuk Theerakulpisut
Khon Kaen University
Manunya Okhawilai
Chulalongkorn University
Pornnapa Kasemsiri (pornkas@kku.ac.th)
Khon Kaen University https://orcid.org/0000-0003-3416-9376

Research Article

Keywords: epoxy nanocomposite, vitrimer, bio-based curing agent, self-healing, anti-corrosion

DOI: https://doi.org/10.21203/rs.3.rs-410734/v1

Abstract

Epoxy is extensively used for anti-corrosion coatings on metallic materials. Conventional epoxy coatings have a permanent crosslink network that is unable to repair itself when cracks and damages occur on the coating layer. This study aims to develop self-healing epoxy vitrimer/carbon nanotube (CNTs) nanocomposite for coating. Two bio-based curing agents viz., cashew nut shell liquid (CNSL) and citric acid (CA) were employed to create covalent adaptable networks. The 0-0.5 wt% CNTs were also incorporated into epoxy/CNSL/CA matrix (V-CNT0-0.5). Based on the results of our study, thermomechanical properties of V-CNT nanocomposites increased with increasing CNTs content. The bond exchange reaction of esterification was thermally activated by near infrared (NIR) light. The V-CNT0.5 showed the highest self-healing efficiency in Shore D hardness of 97.37%. The corrosion resistance of coated steel with V-CNT0 and V-CNT0.5 were observed after immersing the samples in 3.5 wt% NaCl for 7 days. The corrosion rate of coated steel with V-CNT0.5 decreased from 9.53×10^{2} MPY to 3.12×10^{-5} MPY whereas an increase in protection efficiency of 99.99% was observed. By taking advantages of the superior self-healing and anti-corrosion properties, V-CNT0.5 could prove to be a desirable organic anti-corrosion coating material.

1. Introduction

Nowadays, organic coatings are widely used in various industries to prevent corrosion of metal surfaces. The organic coatings have attracted much attention to replace heavy metals for corrosion prevention due to environmental concerns and safety (1–3). Epoxy is one of organic coating materials used in industry because of its effectiveness and ease of application (4,5). However, defects such as cracks and pores of epoxy coatings during application may result in direct contact between the metal surface and the prevailing aggressive environment leading to corrosion (6). Recently, smart polymers for coatings with self-healing properties have been developed to prolong service life and reduce maintenance cost of materials (7). Vitrimers are smart thermosets that have cross-linked polymer networks with reversibility through thermally activated bond exchange reactions (BERs) (8,9). The exchange reactions allow vitrimers to rearrange their topology leading to the abilities of reshaping, welding, healing and reprocessing via thermal treatment (10). Jouyandeh et al. (11) studied organic coatings based on epoxy vitrimer nanocomposites containing modified cellulose with halloysite nanotubes (HNT-C). The epoxy containing 0.3 wt% HNT-C showed a good self-healing behavior with an approximately 56% increase in tensile strength compared to neat epoxy.

Bio-based curing agents for epoxy have become a topic of interest because of their biocompatibility and eco-friendliness (12,13). Cashew nut shell liquid (CNSL) is an inexpensive bio-based curing agent for epoxy that is obtained as the by-product of cashew nut production (14–17). Three main components of CNSL are cardanol, cardol and anacardic acid. The two main kinds of crosslinked networks between epoxy and CNSL are ether and ester linkages (16). Kasemsiri et al. (12) studied the properties of epoxy phenolic novolac (EPN) cured with CNSL, and the shape reconfigurability and self-welding properties of the vitrimer were observed. However, the reconfigured shape of EPN/CNSL composite could not

completely be fixed due to insufficient ester linkages. Esterification in the epoxy network can be promoted by adding natural carboxylic acids such as citric acid (CA). A vitrimer from epoxy cured with CA and catalyzed by imidazole had 99% reconfigurability of new shape after heating at 160 °C for 1 h via transesterification (18). Based on previous studies (12,18), the use of epoxy cured with bio-based curing agents such as CNSL combined with CA presents an attractive smart polymer candidate for organic coatings.

To improve properties and create new functions for specific coating applications, the incorporation of nanoparticles viz., carbon nanotubes (CNTs) into epoxy matrices has been reported (19,20). CNTs have mild chemical stability, high electrical conductivity, and good mechanical properties (21). Deyab and Awadallah (22) observed that adding CNTs into epoxy can reduce corrosion rates by forming uniform coating layers. The resistance from equivalent electric circuits showed that epoxy containing CNTs had an electrical resistance value that was 11-20 times greater than neat epoxy. The incorporation of CNTs into polymer matrices not only improves anticorrosion but also enhances the self-healing ability of polymer coatings. The healing process of most self-healing CNTs incorporated polymers can be activated by heat and near infrared (NIR) light (12,23). CNTs are photothermal fillers that can convert the absorbed NIR light into heat. Guan et al (24) studied the self-healing ability of epoxy cured with 4-aminophenyl disulfide (EP-AFD) containing CNTs. They found that self-healing efficiency of EP-AFD containing CNTs increased from 85% to 90% when the temperature was increased from 130^{o}C to 160^{o}C during NIR irradiation for 1 min.

To our knowledge, there have been only few reports on the properties of vitrimer nanocomposites based on the use of bio-based curing agents and CNTs for coating application. Therefore, the aims of this study were to develop novel bio-based vitrimer based epoxy cured with CNSL and CA and incorporated with CNTs. The curing reactions, thermomechanical properties, NIR light-activated self-healing and anticorrosion efficiency were investigated.

2. Experimental

2.1 Materials

Epotec YD 128® Bisphenol A diglycidyl ether (DGEBA) epoxy was provided by Aditya Birla Chemicals (Thailand) with an epoxy equivalent weight (EEW) of 185-194 g eq^{-1}. The CNSL (36.2% cardol, 31.5% cardanol, and 24.6% anacardic acid and trace amount of 2-methyl cardol) was purchased from Mahboonkrong Sirichai 25 Ltd., Nakhon Ratchasima, Thailand. Citric acid monohydrate (AR grade) with an acid equivalent weight (AEW) of 70 g eq^{-1} and ethanol were purchased from RCI Labscan. US4308 COOH functionalized multi-walled carbon nanotubes (CNTs, purity > 95% and outer diameter 10-20 nm) were supplied by US Research Nanomaterials, Inc. The composition of the steel plate was characterized using optical emission spectrometer (Thermo Scientific, ARL 3460) as listed in Table S1. The steel plate was polished using sandpaper (No. 600) for 100 times and then rinsed with acetone.

2.2 Preparation of vitrimer nanocomposites

The epoxy/CNSL/CA matrices at various equivalent ratios of AEW of CA to EEW (R ratio) were prepared for preliminary test of self-healing efficiency, as summarized in Table S2. The CA was dissolved in ethanol and then mixed with CNSL for 10 min using a magnetic stirrer. The epoxy was added into the mixture of CA and CNSL and then stirred for another 10 min. The obtained solution was casted onto the steel plate using doctor blade. The sample was cured at 60, 80, 100, and 120 °C for 1 h each followed by 200 °C for 2 h. The suitable epoxy/CNSL/CA was found at R ratio of 0.35 as depicted in Figure S1. This R ratio showed the self-healing on surface without any scratch and was subsequently used to prepare the vitrimer nanocomposites for coating.

For vitrimer nanocomposite preparation, the CNTs were dispersed in ethanol for 5 min by probe sonication using a UCD-P01-250W ultrasonic cell disrupter from Biobase Biodustry (Shandong) Co., Ltd. Sonication was done at 50 % vibration amplitude with 3-s on and 1-s off pulses. The CNTs/ethanol suspension was mixed with the CA/CNSL solution and stirred for 5 min. The resulting CNT/CA/CNSL suspension in ethanol was mixed with epoxy for 15 min by sonication and stirred for another 30 min. Finally, the obtained mixture was casted on the steel plate and cured in an air-circulated oven following the heating steps as described above. The thickness of the prepared coatings on the steel plates was 200±35 μm. The vitrimer nanocomposites with CNTs contents of 0, 0.1, 0.3, and 0.5 wt%, were named as V-CNT0, V-CNT0.1, V-CNT0.3, and V-CNT0.5, respectively.

2.3 Characterization

Attenuated total reflectance-Fourier transform infrared (ATR-FTIR) spectrometry (Tensor 27, Bruker) was carried out in absorbance mode. The wavelength ranged from 4000 to 600 cm^{-1} at a resolution of 4 cm^{-1} over 32 scans. Dynamic mechanical analysis (DMA) was conducted using TA Q800 dynamic mechanical analyzer to study the thermomechanical properties. The size of the nanocomposite films for all DMA tests was 30 mm × 5 mm × 0.7 mm. The multi-frequency-strain tension mode was used at a frequency of 1 Hz and 0.01% strain from -30 to 120 °C with a heating rate of 2 °C min^{-1}. The stress relaxation mode was applied with 0.1% strain at different temperatures, which were 70, 80, 90, and 100 °C. The cross-sectional morphologies of the samples were observed using a field emission scanning electron microscope (FEI Helios NanoLab G3 CX). To evaluate the self-healing ability, the nanocomposite specimens were scratched using a razor blade with 10 μm edge width and exposed to NIR light (120 W, EVE) with light intensity of 1.6 $mW{\cdot}cm^{-2}$ for 1 h. The images of the specimens before and after NIR light exposure were taken using a Nikon Measurescope 20 stereo microscope and analyzed by ImageJ software for the change in the size of the scratch. The self-healing ability was calculated using Eq. 1.

$$\text{Self-healing ability} = \frac{L_h - L_i}{L_i} \times 100\% \qquad (1)$$

where L_i refers to an initial width of the damaged area and L_h represents the width after healing for different healing times.

Shore D hardness tests were performed on the vitrimer coating using a handheld durometer according to ASTM D2240 (25). The self-healing efficiency of the coatings was calculated using Eq. 2.

$$\text{Self-healing efficiency of coating} = \frac{\text{Hardness value after healing}}{\text{Initial hardness value}} \times 100\% \qquad (2)$$

Electrochemical corrosion tests were performed using a palmsen.4 electrochemical workstation with three electrodes. Platinum and silver/silver chloride were used as auxiliary electrode and reference electrode, respectively, while the coated sample with exposure area of 0.283 cm^2 functioned as working electrode. The sample was immersed in 3.5 wt% NaCl aqueous solution. Potentiodynamic curves were collected at a scan rate of 0.005 $mV.s^{-1}$. X-ray diffraction (XRD) analyses were performed using PANalytical, EMPYREAN at 2θ = 20°–80° with a step of 0.02°, voltage of 45 kV, and current of 40 mA.

3. Results And Discussion

3.1 Characterization of chemical structure

The FTIR spectra of V-CNT containing different CNTs contents are displayed in Figure 1. The mixture of epoxy/CNSL/CA before curing is depicted in Figure 1(a). The main characteristic peak of epoxy was observed at 915 cm^{-1}, which was attributed to epoxide rings. The C–H and C–CH_2 stretching vibrations of epoxide rings were also found at 2864 and 1453 cm^{-1}, respectively (26). The absorption bands at 1007 and 912 cm^{-1} were assigned to the phenolic group of CNSL. The C=O stretching of citric acid and anacardic acid appeared at 1650 cm^{-1} (16,27). Figure 1(b) shows FTIR spectra of samples after the curing process. All samples display similar FTIR spectra. The peak intensity at 915 cm^{-1} remarkably decreased, which indicates the opening of the epoxide rings followed by crosslinking (16). The peak at 1734 cm^{-1} was assigned to C□O stretching of ester, which was formed by esterification between epoxy and the carboxyl groups of CA and anacardic acid (28). The 1112 cm^{-1} peak was attributed to C—O—C stretching of ether, which confirms the etherification between epoxy and hydroxyl groups of cardanol and cardol in CNSL (29). Figure 1(c) shows the peak shift from 3444 cm^{-1} to 3436 cm^{-1} after adding CNTs at various contents. This shift was due to H-bonding interaction between C□O group of CNTs and the OH groups of epoxy matrix during the ring opening polymerization reaction (30). The possible reactions of epoxy, CNSL, CA and CNTs are depicted in Scheme S1.

3.2 Thermomechanical properties of vitrimer nanocomposites

The relationships between storage modulus and temperature of V-CNT are revealed in Figure 2. The storage moduli at glassy state (0 °C) of V-CNT0, V-CNT0.1, V-CNT0.3, and V-CNT0.5 vitrimers were 5773,

6658, 7366 and 8602 MPa, respectively. This increase in storage modulus with increasing CNTs content was attributed to the reinforcing effect of the homogeneous dispersion of CNTs nanofiller (12). The cross-sectional micrographs of all samples were used to confirm the dispersion of CNTs without aggregation as shown in Figure 3. Saha and Bal (31) suggested that the carboxylic groups on CNTs could form covalent bonds with epoxy which enhanced the interfacial stress transfer and positively improved dispersability of CNTs. Figure 4 depicts the Tg which was determined from the peak loss modulus. The Tg of the V-CNT increased from 27.3 to 30.6 °C when 0-0.5 wt% CNTs were incorporated in the epoxy matrix. The increase in CNTs content improved the glassy storage modulus and Tg of the nanocomposites, which could be explained by the effect of CNTs reinforcement. Uniformly dispersed CNTs in the network obstructed the mobility of the polymer chains, leading to a higher resistance for deformation (32). Furthermore, the strong covalent bonding between epoxy and COOH groups on CNTs promoted dissipation of energy between CNTs and matrix, enhancing the thermal properties of the epoxy composite (30).

3.3 Stress relaxation of vitrimer nanocomposites

Figure 5 depicts the relationship between the normalized relaxation modulus (G/G0) and time at 70, 80, 90, and 100 °C for the V-CNT specimens with different CNTs contents. A relaxation time for viscoelastic fluid can be defined at the G/G0 of 0.37, according to Maxwell model (33). It can be observed that all specimens can reduce the G/G0 value to 0.37, indicating the completion of BER via esterification to transesterification in the specimens. Figure 6(a) shows the linear relationship between relaxation time and temperature. The transesterification activation energy can be obtained from the slope of the plot according to Eq. 3 (34). Moreover, the topology freezing transition temperature (Tv) of the vitrimer can be evaluated at ln(t*) value of 13.8 via extrapolation (35,36).

$$\ln(t^*) = E_a / RT + \ln(t_0) \qquad (3)$$

where t* is relaxation time (s), T is temperature (K), E_a is the activation energy (kJ/mol), and R is the universal gas constant.

Legrand and Soulié-Ziakovic (37) suggested that the stress relaxation of vitrimers containing functionalized fillers depended on two main phenomena, i.e. (i) the bond exchange of linkages between filler and polymer matrix and rearrangement and (ii) rearrangement of the filler in the polymer matrix. Figure 6(b) shows the activation energy and Tv of V-CNT with different CNTs contents. The E_a values ranged from 55.7 to 62.4 kJ/mol and increased with CNTs content. The increase of CNTs in the network hindered the polymer chain mobility, hence a higher energy was required for transesterification. This observation was in good agreement with a previous report on polymethacrylate vitrimer nanocomposites (38). The Tv values of V-CNT0-0.5 were in the range of -26.1 to -12.0 °C. This Tv was also observed to increase with CNTs in the specimens, which was related to the hindrance effect of CNTs on the chain mobility. The delay in transesterification rate due to the increasing CNTs therefore led to the increase in Tv (39).

3.4 NIR Self-healing ability of vitrimer nanocomposites

Dynamic thermosetting is a new class of polymers that has been developed to resolve the limitations (unrepairable and unrecyclable) of conventional thermosetting polymers. Figure 7 demonstrates the self-healing ability of V-CNT specimens before and after NIR exposure. After NIR exposure for 1 h, the scratch sizes were obviously reduced, particularly for V-CNT0.5. Since the photo-activation resulted in a higher thermal energy, transesterifications in the vitrimer network were initiated to dissociate the crosslinked network. This phenomenon allows the polymer chain diffusion to fill the scratch, resulting in self-healing (40). Without CNTs, the V-CNT0 showed self-healing because of the □-□ interactions between polymer chains (41), but the self-healing ability was only 31%. The addition of CNTs improved self-healing ability of V-CNT up to 93%, three times as high as that of V-CNT0, as shown in Figure 8. The addition of CNTs in the vitrimer network directly promoted the photothermal conversion effect, leading to the higher thermal energy activating transesterifications (42). In addition, CNTs promoted heat dissipation in the polymer matrix to improve heat transfer throughout the network, according to their high thermal conductivity (43). Previously it was reported that an increase in CNTs content in the composites could physically retard the chain mobility, resulting in poor self-healing ability (44). The self-healing results in this work demonstrate the opposite, which is likely due to the functionalization of the CNTs. The CNTs in this work contain COOH groups, which increase the compatibility to bond with epoxide groups to create reversible linkages that participate in the self-healing process (45,46).

3.4 Self-healing efficiency of vitrimer nanocomposite coating

The Shore D hardness was measured to investigate the ability of the coatings to resist indentation using a durometer scale in range of 0-100, as shown in Table 1. A higher value represents a harder coating material. The hardness values of virgin samples increased with CNTs content and ranged from 27.53 to 30.13, which were comparable to those of bio-based epoxy cured with anhydride and organic acids (47) and epoxy/polycaprolactone copolymer (48). After healing, the hardness values slightly decreased for all samples. The self-healing efficiency of the coating increased from 94.34% for coated steel with V-CNT0 to 97.37% for coated steel with V-CNT-0.5. It is postulated that adding CNTs into the epoxy matrix was beneficial to the self-healing efficiency. Since V-CNT0.5 exhibited the highest performance of self-healing in coating, the vitrimer with this composition was used to coat steel plates for anti-corrosion tests.

3.5 Corrosion properties of vitrimer nanocomposite coating

Figure 9 illustrates the Tafel plots of bare steel and steel samples coated with V-CNT-0 and V-CNT-0.5 after immersion in 3.5 wt% NaCl for 7 days. The current (I_{corr}), corrosion potential (E_{corr}), protection efficiency (P.E.) and corrosion rate (R_{corr}) from the Tafel plots are summarized in Table 2. The P.E. and R_{corr} values can be evaluated following Eq. 4 and Eq. 5 (49).

$$P.E(\%) = \left(\frac{I^{o}_{corr} - I^{c}_{corr}}{I^{o}_{corr}} \right) \times 100 \qquad \text{Eq. 4}$$

where I^{0}_{corr} and , I^{c}_{cor} (ampere cm^{-2}) are the corrosion current of steel plate and coated steel plate with vitrimer nanocomposite, respectively.

$$R_{corr}(MPY) = \frac{I_{corr} \cdot KE_{w}}{d \cdot A} \qquad \text{Eq. 5}$$

where R_{corr} is corrosion rate in milli-inches per year (MPY), E_w is equivalent weight of sample (g $equivalent^{-1}$), K is a constant value (1.288×10^5 milli-inches per year/ ampere -cm-year), A is the surface area of sample (cm^2), d is density of the sample (g cm^{-3}) and is the corrosion current (ampere).

The two main parameters, I_{corr} and E_{corr}, were used to analyze the anticorrosion performance. The I_{corr} represents a corrosion dynamic rate involving the cathodic reduction of oxygen and anodic dissolution of metal ions whereas E_{corr} indicates the corrosion resistance performance (50). The negative shift of I_{corr} and positive shift of E_{corr} implies the enhancement in corrosion resistance with low corrosion dynamic rate (51). The anticorrosion performance was in the following order: coated steel with V-CNT0.5 > coated steel with V-CNT0 > uncoated steel. The higher P.E. and lower R_{corr} of coated steel with V-CNT0.5 were also observed. The hydrophobic character of V-CNT0.5 (see supplementary information in Figure S2) repelled the NaCl solution, resulting in diffusion away from the steel substrate. In addition, the uniform dispersion of CNTs can change and hinder the diffusion pathway of oxygen molecules, chlorine ions and H_2O molecules in the epoxy matrix (50). Harb et al (52) suggested that the negatively charged CNTs in a polymer matrix acted as a repulsive agent for chloride anions resulting in an increase in ionic resistance. Furthermore, the presence of CNTs with high aspect ratio increased the surface area for oxygen cathodic half reaction resulting in a decrease in over-potential for the reduction of oxygen molecule. At a low over-potential, the passive film formation might occur due to an increased metal dissolution at the anode in low corrosion current density (53).

The corrosion products of steel coated with V-CNT0 and V-CNT0.5 after immersion in 3.5 wt% NaCl solution for 7 days were characterized using XRD, as shown in Figure 10. The main corrosion products of coated steel V-CNT0 and V-CNT0.5 were found at 28.8° (Fe_3O_4), 30.1 ° ($Fe_2(OH_3)Cl$), 35.4 ° (α-FeOOH), 43.2 ° (Fe), 57.1 ° (Fe_3O_4) and 63.5 ° (Fe). Differently, the peak at 31.9° (Fe_2O_3) was only observed in the steel coated with V-CNT0.5. The Fe_3O_4 peaks were derived from the steel substrate and corrosion products (6,54). This oxide film acted as a barrier to prevent oxygen from invading into the mediate layer (54). The proposed corrosion protection mechanism of the steel coated with V-CNT0 and V-CNT0.5 is illustrated in Scheme 1.

Conclusion

In this work, epoxy vitrimer nanocomposites were successfully developed and applied as anticorrosion coatings. The prepared epoxy vitrimer at R=0.35 provided a uniform and self-healing coating film. Hence, this epoxy vitrimer formula was used to prepare vitrimer nanocomposites. The incorporation of CNTs at 0-0.5 wt% enhanced the storage modulus from 5773 MPa to 8602 MPa and increased the Tg from 27.3 °C to 30.6 °C. The V-CNT0.5 showed the highest self-healing ability of 93%. The Shore D hardness increased from 27.53 to 30.12 when 0.5 wt% CNTs was incorporated into the epoxy matrix. After healing, V-CNT0.5 showed the highest Shore D hardness of 29.33. The uniform dispersion of CNTs in the epoxy matrix improved the BER capability under NIR light irradiation. The coated steel with V-CNT0.5 showed good anti-corrosion performance, which decreased the corrosion rate from 9.53×10^{2} MPY to 3.12×10^{-5} MPY. Based on the obtained results, the V-CNT0.5 has good potential to be used as an organic anti-corrosion coating.

Declarations

Acknowledgement

This work was supported by the Royal Golden Jubilee Ph.D. scholarship of the Thailand Research Fund [grant number PHD/0172/2559] and the Applied Engineering for Important Crops of the North East Research Group Khon Kaen University, Thailand.

References

1. Hegde MB, Nayak SR, Mohana KNS, Swamy NK (2020) Garcinia gummigutta Vegetable Oil–Graphene Oxide Nano-composite: An Efficient and Eco-friendly Material for Corrosion Prevention of Mild Steel in Saline Medium. J Polym Environ 28(2):483–99.
2. Alam M, Alandis NM, Ahmad N (2020) Corn oil-derived poly (urethane-glutaric-esteramide)/fumed silica nanocomposite coatings for anticorrosive applications. J Polym Environ 28(3):1010–20.
3. Ataei S, Hassan A, Yahya R (2021) Dual Microcapsulation of an Environmentally-Friendly-Based Reactive Multifunctional Acrylated Epoxy Resin and Thiol by Internal Phase Separation Technique for Self-healing Applications. J Polym Environ 1–15.
4. Shen W, Zhang T, Ge Y, et al (2021) Multifunctional AgO/epoxy nanocomposites with enhanced mechanical, anticorrosion and bactericidal properties. Prog Org Coatings 152:106130.
5. Feng L, He X, Zhang Y, et al (2021) Triple Roles of Thermoplastic Polyurethane in Toughening, Accelerating and Enhancing Self-healing Performance of Thermo-reversible Epoxy Resins. J Polym Environ 29(3):829–36.
6. Ye Y, Yang D, Zhang D, et al. (2020) POSS-tetraaniline modified graphene for active corrosion protection of epoxy-based organic coating. Chem Eng J 383:123160.

7. Patil AM, Gite V V, Jirimali HD, Jagtap RN (2021) Fully Biobased Nanocomposites of Hyperbranched-Polyol and Hydroxyapatite in Coating Applications. J Polym Environ 29(3):799–810.
8. Solouki Bonab V, Karimkhani V, Manas-Zloczower I (2019) Ultra-Fast Microwave Assisted Self-Healing of Covalent Adaptive Polyurethane Networks with Carbon Nanotubes. Macromol Mater Eng 304(1):1800405.
9. Yang X, Guo L, Xu X, et al (2020) A fully bio-based epoxy vitrimer: Self-healing, triple-shape memory and reprocessing triggered by dynamic covalent bond exchange. Mater Des 186:1–10.
10. Denissen W, Winne JM, Du Prez FE (2016) Vitrimers: permanent organic networks with glass-like fluidity. Chem Sci 7(1):30–8.
11. Jouyandeh M, Tikhani F, Hampp N, et al (2020) Highly curable self-healing vitrimer-like cellulose-modified halloysite nanotube/epoxy nanocomposite coatings. Chem Eng J 396:125196.
12. Kasemsiri P, Lorwanishpaisarn N, Pongsa U, Ando S (2018) Reconfigurable Shape Memory and Self-Welding Properties of Epoxy Phenolic Novolac/Cashew Nut Shell Liquid Composites Reinforced with Carbon Nanotubes 10:482.
13. Shnawa HA (2020) Curing and thermal properties of tannin-based epoxy and its blends with commercial epoxy resin. Polym Bull 1–16.
14. Meng H, Li G (2013) A review of stimuli-responsive shape memory polymer composites. Polymer (Guildf) 54(9):2199–2221.
15. Lorwanishpaisarn N, Kasemsiri P, Jetsrisuparb K, et al (2019) Dual-responsive shape memory and self-healing ability of a novel copolymer from epoxy/cashew nut shell liquid and polycaprolactone. Polym Test 81:106159.
16. Kasemsiri P, Neramittagapong A, Chindaprasirt P (2015) Curing kinetic, thermal and adhesive properties of epoxy resin cured with cashew nut shell liquid. Thermochim Acta 600:20–7.
17. Lorwanishpaisarn N, Kasemsiri P, Srikhao N, et al (2019) Fabrication of durable superhydrophobic epoxy/cashew nut shell liquid based coating containing flower-like zinc oxide for continuous oil/water separation. Surf Coatings Technol 366:106–13.
18. Altuna FI, Hoppe CE, Williams RJJ (2016) Shape memory epoxy vitrimers based on DGEBA crosslinked with dicarboxylic acids and their blends with citric acid. RSC Adv 6(91):88647–55.
19. Mittal G, Dhand V, Rhee KY, et al (2015) A review on carbon nanotubes and graphene as fillers in reinforced polymer nanocomposites. J Ind Eng Chem 21:11–25.
20. He X, Lin S, Feng X, Pan Q (2021) Synthesis and Modification of Polyurethane Foam Doped with Multi-walled Carbon Nanotubes for Cleaning up Spilled Oil from Water. J Polym Environ 29(4):1271–86.
21. Gusmão AP, Rosenberger AG, Muniz EC, et al (2020) Characterization of Microfibers of Carbon Nanotubes Obtained by Electrospinning for Use in Electrochemical Sensor. J Polym Environ 1–15.
22. Deyab MA, Awadallah AE (2020) Advanced anticorrosive coatings based on epoxy/functionalized multiwall carbon nanotubes composites. Prog Org Coatings 139:105423.

23. Wang F, Zhang C, Wan X (2021) Carbon Nanotubes-Coated Conductive Elastomer: Electrical and Near Infrared Light Dual-Stimulated Shape Memory, Self-Healing, and Wearable Sensing. Ind Eng Chem Res 60(7):2954–2961.
24. Liu H, Zhao W, Gao G, Ren X (2019) Tough, anti-freezing and non-drying double network organohydrogels. Mater Today Commun 21:100609.
25. ASTM D2240 (2010) Standard Test Method for Rubber Property , American Society for Testing and Materials: West Conshohocken, PA
26. Baig Z, Akram N, Zia KM, et al (2020) Influence of amine-terminated additives on thermal and mechanical properties of diglycidyl ether of bisphenol A (DGEBA) cured epoxy. J Appl Polym Sci 137(8):48404.
27. Bai Y, Chen X (2017) A fast water-induced shape memory polymer based on hydroxyethyl cellulose/graphene oxide composites. Compos Part A Appl Sci Manuf 103:9–16.
28. Xu S, Girouard N, Schueneman G, et al (2013) Mechanical and thermal properties of waterborne epoxy composites containing cellulose nanocrystals. Polymer (Guildf) 54(24):6589–98.
29. Hager MD, Bode S, Weber C, Schubert US (2015) Shape memory polymers: Past, present and future developments. Prog Polym Sci 49–50:3–33.
30. Gogoi P, Horo H, Khannam M, Dolui SK (2015) In situ synthesis of green bionanocomposites based on aqueous citric acid cured epoxidized soybean oil-carboxylic acid functionalized multiwalled carbon nanotubes. Ind Crops Prod 76:346–54.
31. Saha S, Bal S (2017) Influence of nanotube content on the mechanical and thermo-mechanical behaviour of –COOH functionalized MWNTs/epoxy composites. Bull Mater Sci 40(5):945–56.
32. Tan C, Zhang W, Wang Q, et al (2019) Viscoelastic behavior of carboxylated multi-walled carbon nanotube reinforced epoxy composites with various frequencies. Mater Res Express 6(9):95305.
33. Wim D, Guadalupe R, Renaud N, et al (2015) Vinylogous urethane vitrimers. Adv Funct Mater 25(16):2451–7.
34. Niu X, Wang F, Li X, et al (2019) Using Zn2+ ionomer to catalyze transesterification reaction in epoxy vitrimer. Ind Eng Chem Res 58(14):5698–706.
35. Zhiyan M, Yan W, Jing Z, et al (2017) Bio-based epoxy vitrimers: Reprocessibility, controllable shape memory, and degradability. J Polym Sci Part A Polym Chem 55(10):1790–9.
36. Capelot M, Unterlass MM, Tournilhac F, Leibler L (2012) Catalytic control of the vitrimer glass transition. ACS Macro Lett 1(7):789–92.
37. Legrand A, Soulié-Ziakovic C (2016) Silica–Epoxy Vitrimer Nanocomposites. Macromolecules 49(16):5893–902.
38. Zhang F, Wu Q, Liu H (2020) NIR light-triggered nanomaterials-based prodrug activation towards cancer therapy. WIREs Nanomedicine and Nanobiotechnology 12(6):e1643.
39. Hajiali F, Tajbakhsh S, Marić M (2020) Thermally reprocessable bio-based polymethacrylate vitrimers and nanocomposites. Polymer (Guildf) 123126.

40. Du W, Jin Y, Shi L, et al (2020) Shen Y, Lai S, Zhou Y. NIR-light-induced thermoset shape memory polyurethane composites with self-healing and recyclable functionalities. Compos Part B Eng 195:108092.
41. Amornkitbamrung L, Srisaard S, Jubsilp C, et al (2020) Near-infrared light responsive shape memory polymers from bio-based benzoxazine/epoxy copolymers produced without using photothermal filler. Polymer (Guildf) 209:122986.
42. Wang H, Yang Y, Zhang M, et al (2020) Electricity-triggered self-healing of conductive and thermostable vitrimer enabled by paving aligned carbon nanotubes. ACS Appl Mater Interfaces 12(12):14315–22.
43. Hassanzadeh-Aghdam MK, Ansari R (2019) Thermal conductivity of shape memory polymer nanocomposites containing carbon nanotubes: A micromechanical approach. Compos Part B Eng 162:167–77.
44. Szatkowski P, Pielichowska K, Blazewicz S (2017) Mechanical and thermal properties of carbon-nanotube-reinforced self-healing polyurethanes. J Mater Sci 52(20):12221–34.
45. Zhou T, Wang X, Zhu H, Wang T (2009) Influence of carboxylic functionalization of MWCNTs on the thermal properties of MWCNTs/DGEBA/EMI-2,4 nanocomposites. Compos Part A Appl Sci Manuf 40(11):1792–7.
46. Guadagno L, Vertuccio L, Naddeo C, et al (2020) Functional structural nanocomposites with integrated self-healing ability. Mater Today Proc 34: 243-249.
47. Thiele K, Eversmann N, Krombholz A, Pufky-Heinrich D (2019) Bio-based epoxy resins based on linseed oil cured with naturally occurring acids. Polymers (Basel) 11(9):1409.
48. Arnebold A, Wellmann S, Hartwig A (2016) Network dynamics in cationically polymerized, crosslinked epoxy resins and its influence on crystallinity and toughness. Polymer (Guildf) 91:14–23.
49. Yu YH, Lin YY, Lin CH, et al (2014) High-performance polystyrene/graphene-based nanocomposites with excellent anti-corrosion properties. Polym Chem 5(2):535–50.
50. Kumar A, Ghosh PK, Yadav KL, Kumar K (2017) Thermo-mechanical and anti-corrosive properties of MWCNT/epoxy nanocomposite fabricated by innovative dispersion technique. Compos Part B Eng 113:291–9.
51. Yao Y, Sun H, Zhang Y, Yin Z (2020) Corrosion protection of epoxy coatings containing 2-hydroxyphosphonocarboxylic acid doped polyaniline nanofibers. Prog Org Coatings 139:105470.
52. Harb S V, Pulcinelli SH, Santilli C V, et al (2016) A comparative study on graphene oxide and carbon nanotube reinforcement of PMMA-siloxane-silica anticorrosive coatings. ACS Appl Mater Interfaces 8(25):16339–50.
53. Shen W, Feng L, Liu X, et al (2016) Multiwall carbon nanotubes-reinforced epoxy hybrid coatings with high electrical conductivity and corrosion resistance prepared via electrostatic spraying. Prog Org Coatings 90:139–46.
54. Rui M, Zhu A (2021) The synthesis and corrosion protection mechanisms of PANI/CNT nanocomposite doped with organic phosphoric acid. Prog Org Coatings 153:106134.

Tables

Table 1 Shore D hardness of steel coated vitrimer nanocomposites.

Samples	Initial hardness value	Hardness value after healing	Self-healing efficiency of coating
V-CNT0	27.53 ± 1.40	26.13 ± 0.29	94.85
V-CNT0.1	27.67 ± 0.76	26.5 ± 1.09	95.78
V-CNT0.3	29.50 ± 0.80	28.5 ± 1.02	96.61
V-CNT0.5	30.13 ± 1.25	29.33 ± 0.97	97.37

Table 2 Electrochemical parameters of steel coated vitrimer nanocomposite after immersing in 3.5 wt% NaCl for 7 days.

Samples	I_{corr} (A/cm^2)	E_{corr} (V)	R_{corr} (MPY)	P_{EF} (%)
Bare steel	0.018	-0.79	9.53×10^{2}	-
Steel coated V-CNT0	6.06×10^{-6}	-0.60	3.46×10^{-1}	99.97
Steel coated V-CNT0.5	5.90×10^{-10}	-0.31	3.12×10^{-5}	99.99

Figures

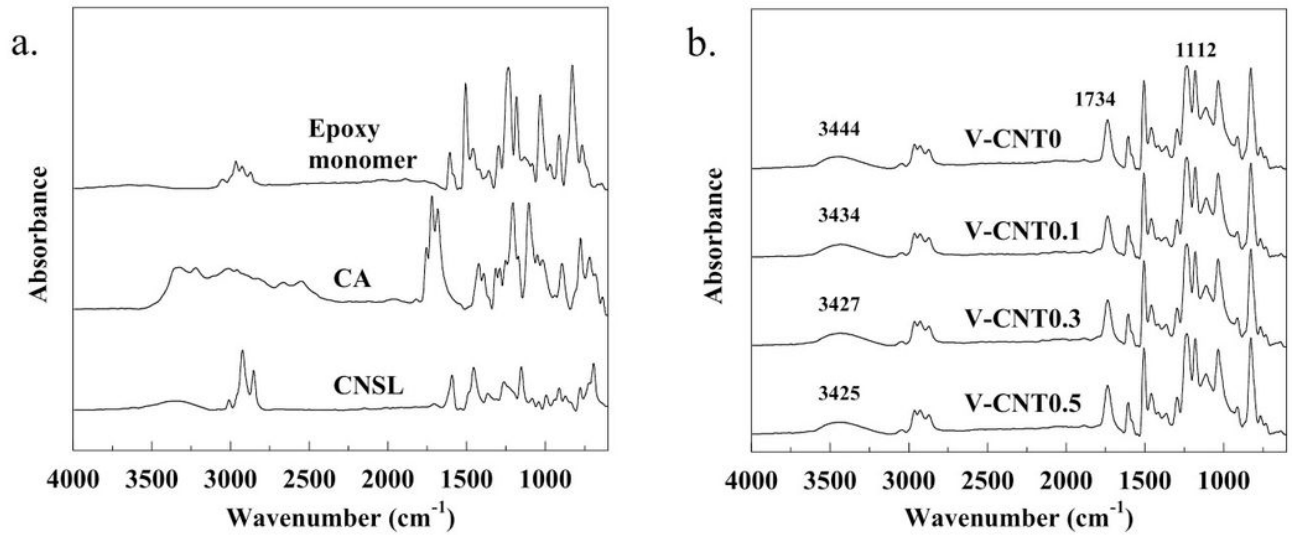

Figure 1

a. The mixture of epoxy/CNSL/CA before curing is depicted. b. The C=O stretching of citric acid and anacardic acid appeared at 1650 cm-1.

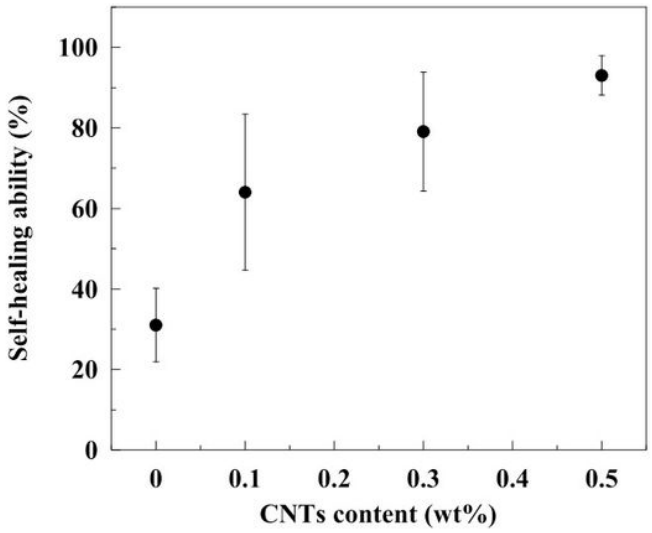

Figure 2

The storage moduli at glassy state (0 °C) of V-CNT0, V-CNT0.1, V-CNT0.3, and V-CNT0.5 vitrimers were 5773, 6658, 7366 and 8602 MPa, respectively.

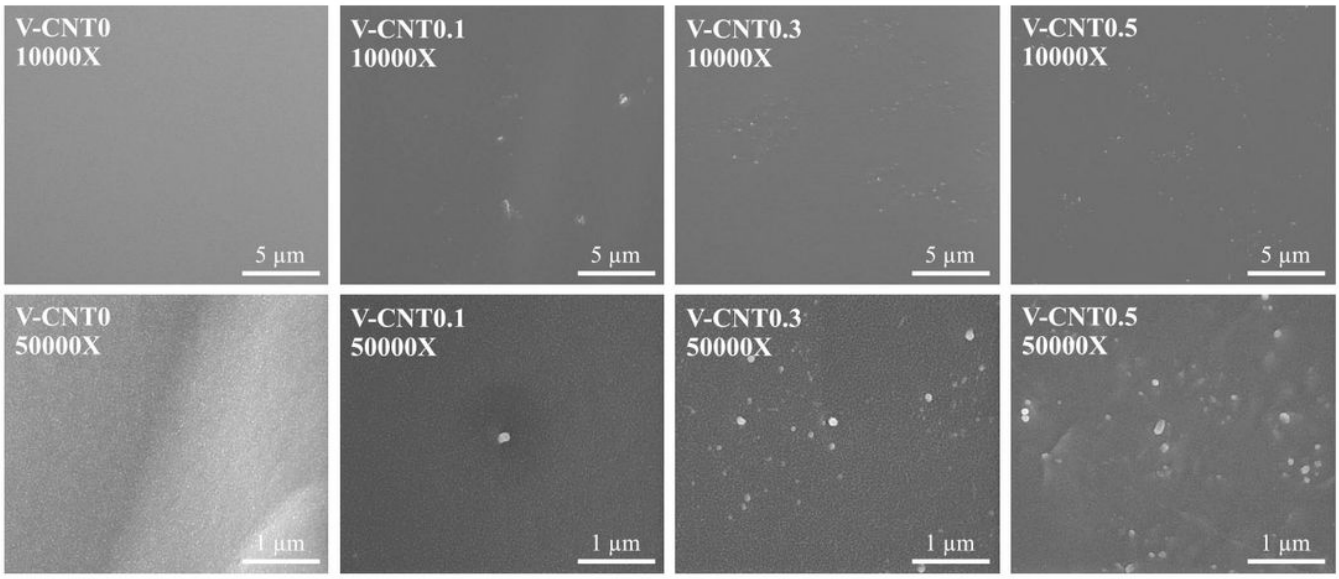

Figure 3

Saha and Bal (31) suggested that the carboxylic groups on CNTs could form covalent bonds with epoxy which enhanced the interfacial stress transfer and positively improved dispersability of CNTs.

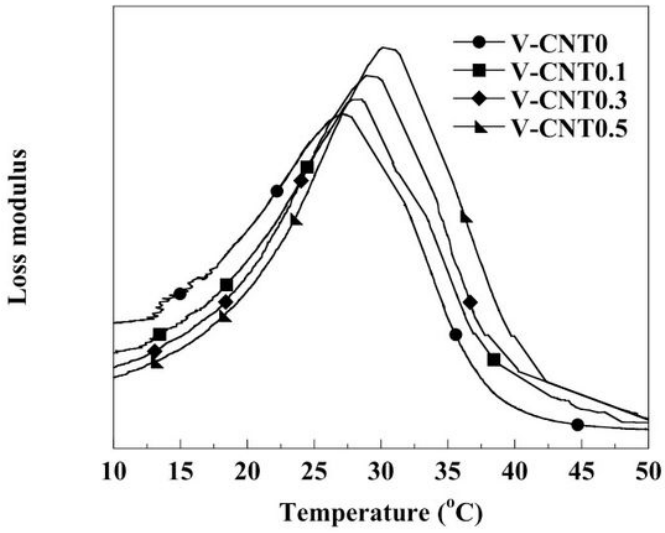

Figure 4

depicts the Tg which was determined from the peak loss modulus. The Tg of the V-CNT increased from 27.3 to 30.6 °C when 0-0.5 wt% CNTs were incorporated in the epoxy matrix.

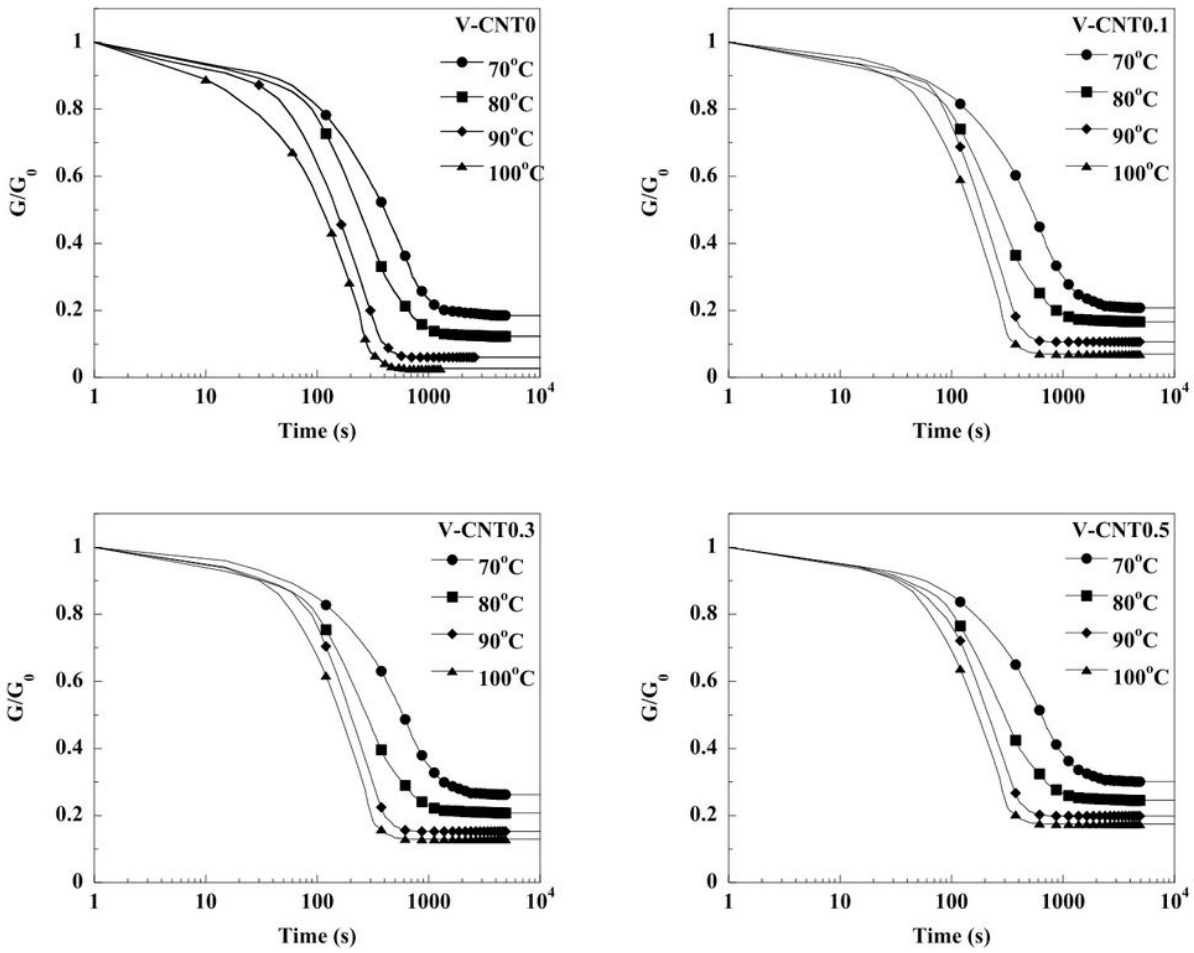

Figure 5

depicts the relationship between the normalized relaxation modulus (G/G0) and time at 70, 80, 90, and 100 °C for the V-CNT specimens with different CNTs contents.

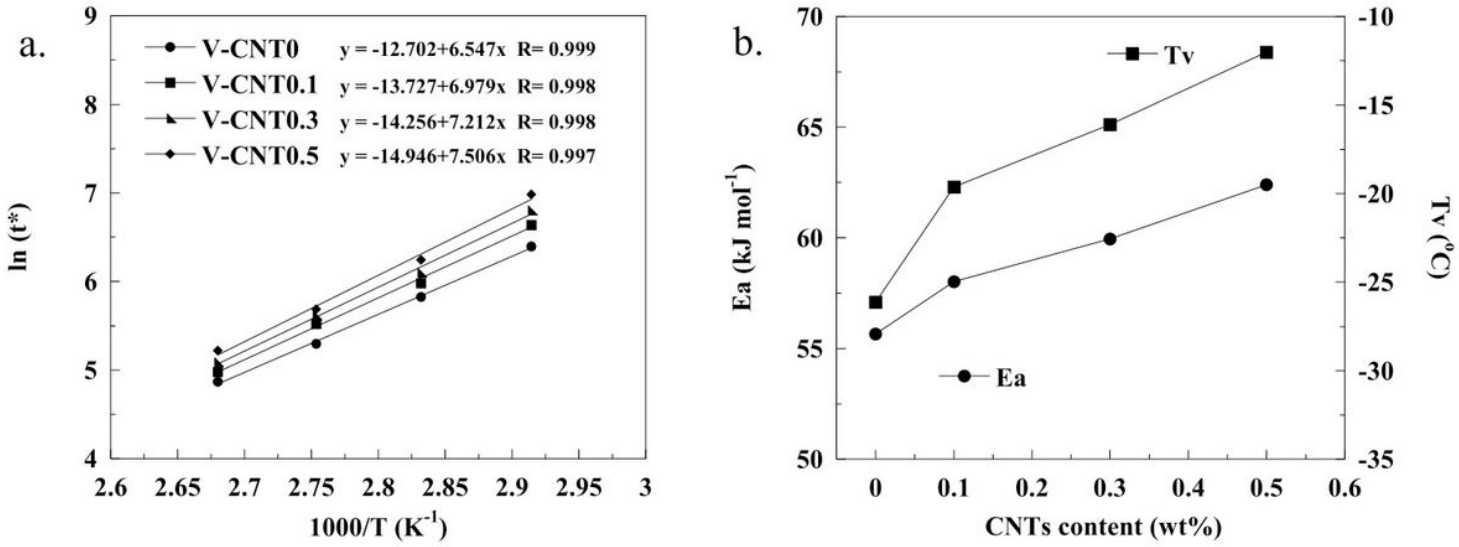

Figure 6

(a) shows the linear relationship between relaxation time and temperature. (b) shows the activation energy and Tv of V-CNT with different CNTs contents.

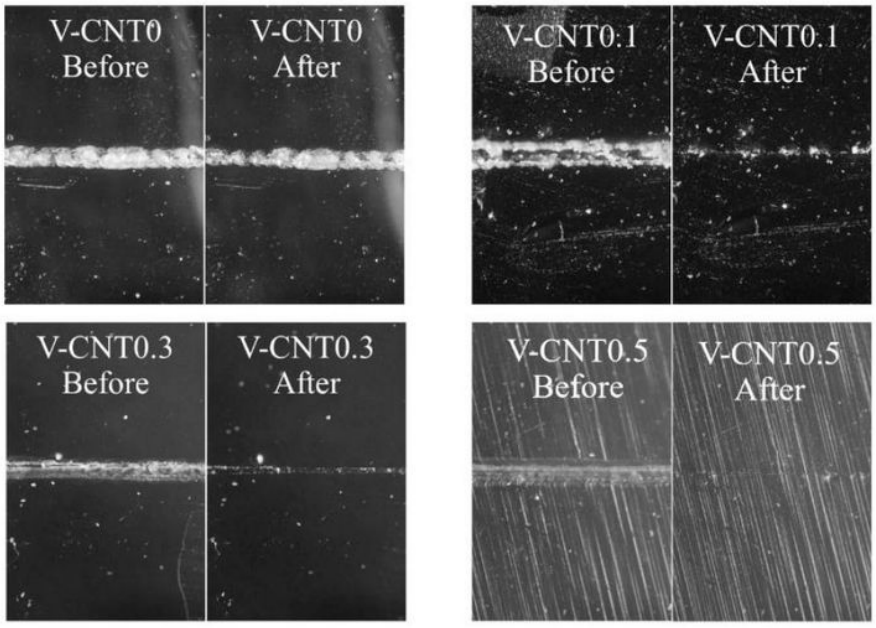

Figure 7

demonstrates the self-healing ability of V-CNT specimens before and after NIR exposure. After NIR exposure for 1 h, the scratch sizes were obviously reduced, particularly for V-CNT0.5. Since the photo-activation resulted in a higher thermal energy, transesterifications in the vitrimer network were initiated to dissociate the crosslinked network.

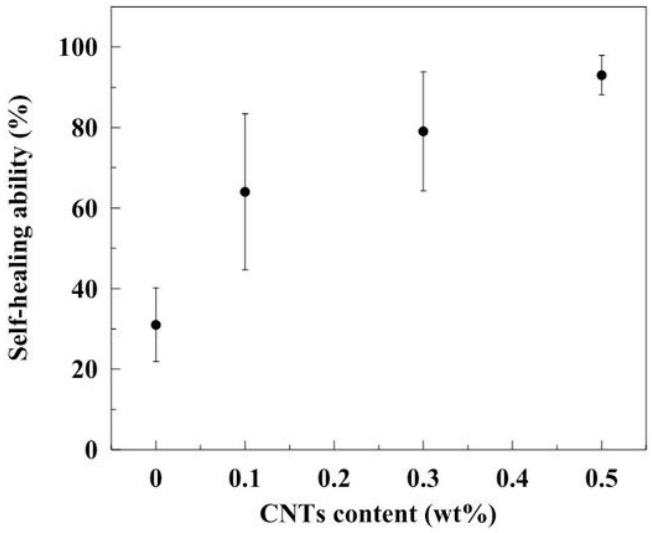

Figure 8

The addition of CNTs in the vitrimer network directly promoted the photothermal conversion effect, leading to the higher thermal energy activating transesterifications (42).

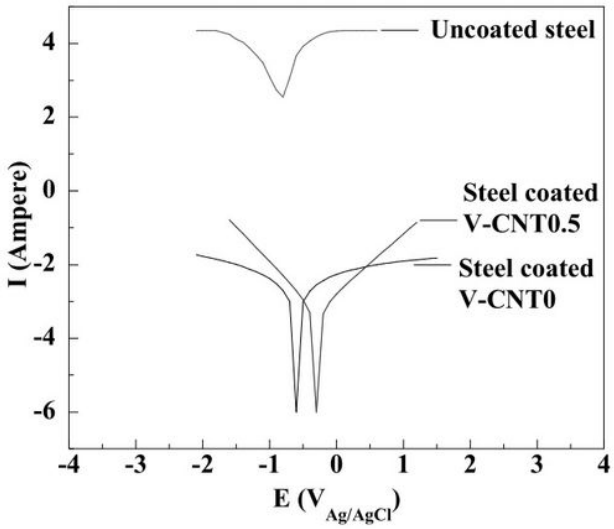

Figure 9

illustrates the Tafel plots of bare steel and steel samples coated with V-CNT-0 and V-CNT-0.5 after immersion in 3.5 wt% NaCl for 7 days. The current (Icorr), corrosion potential (Ecorr), protection efficiency (P.E.) and corrosion rate (Rcorr) from the Tafel plots are summarized in Table 2. The P.E. and Rcorr values can be evaluated following Eq. 4 and Eq. 5 (49).

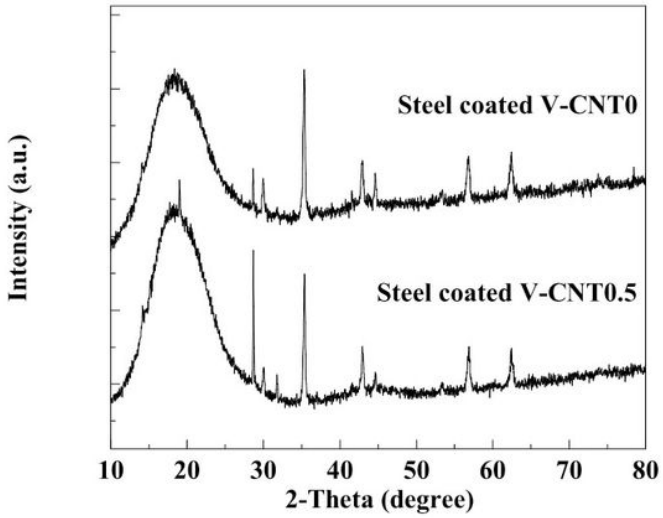

Figure 10

The corrosion products of steel coated with V-CNT0 and V-CNT0.5 after immersion in 3.5 wt% NaCl solution for 7 days were characterized using XRD

Supplementary Files

This is a list of supplementary files associated with this preprint. Click to download.

- 3SupplementaryKasemsirietal.docx
- Scheme1.tif